Acta Mech
https://doi.org/10.1007/s00707-026-04755-w

ORIGINAL PAPER

İsa Çömez

Contact mechanics of porous materials under frictional cylindrical indentation

Received: 26 March 2026 / Revised: 21 April 2026 / Accepted: 7 May 2026
© The Author(s) 2026

Abstract This study presents an analytical investigation of the contact problem involving a porous elastic layer subjected to indentation by a rigid cylindrical punch. In order to obtain a more realistic mechanical representation, frictional interactions at the interface between the punch and the porous layer are incorporated into the formulation. The influence of voids on the linear elastic response of the material is modeled within the framework of the Cowin–Nunziato micro-dilatation theory. The porous layer is assumed to be fully bonded to a rigid foundation. By means of the Fourier transform technique, the governing plane contact problem is reduced to a Cauchy-type singular integral equation of the second kind, wherein the contact stress components and the contact width constitute the primary unknowns. The resulting singular integral equation is solved numerically by employing the Gauss–Jacobi quadrature scheme. Numerical results are presented in graphical form to illustrate the distributions of contact stresses, in-plane stresses, and vertical displacements beneath the rigid punch.

1 Introduction

Porous materials are widely used in modern engineering applications due to their lightweight structure, energy absorption capability, permeability, and tunable mechanical behavior. They are encountered in geomechanics, biomedical implants, filtration systems, thermal insulation components, impact-absorbing layers, and advanced functionally graded structures. The presence of voids significantly alters the mechanical response of these materials compared to classical homogeneous solids. In particular, stress distribution, stiffness degradation, and deformation patterns are strongly influenced by porosity. Therefore, understanding the contact behavior of porous materials under localized loading is of fundamental and practical importance in many technological applications where surface interactions govern performance.

Several theoretical models have been proposed to describe the mechanical behavior of porous materials. One of the most prominent is the consolidation theory introduced by Biot and Willis [1], which was developed to model fluid-saturated porous solids by considering the coupled interaction between the solid matrix and the pore fluid. In the absence of pore fluid, such formulations typically reduce to the equations of classical elasticity,however, Biot's consolidation theory is not applicable to materials containing dry voids, since it fundamentally relies on fluid–solid coupling mechanisms. In contrast, the micro-dilatation theory originally developed by Mindlin [2] and later extended by Nunziato and Cowin [3] and Cowin and Nunziato [4] offers a different and more suitable framework for elastic media with voids. In this approach, the conventional displacement field and the variation in the volume fraction of voids—referred to as micro-dilatation—are treated as independent kinematic variables in the constitutive relations. By incorporating the coupling between

İsa Çömez (✉)
Civil Engineering Department, Karadeniz Technical University, 61080 Ortahisar-Trabzon, Turkey
e-mail: isacomez@hotmail.com; isacomez@ktu.edu.tr

Published online: 25 May 2026

the deformation of the porous matrix and the evolution of void volume fraction during loading, the micro-dilatation theory provides a more comprehensive and physically consistent representation of the mechanical response of dry porous materials. Consequently, for contact mechanics problems involving dry porous layers, the micro-dilatation theory offers a more suitable and physically consistent modeling approach.

The mechanics of porous materials within the framework of the Cowin–Nunziato linear theory have been extensively studied using a wide range of analytical and numerical approaches. These investigations include high-resolution finite element modeling [5], combined analytical and finite element methods [6], continuum-based formulations [7, 8], mixed collocation finite element techniques [9], the meshless Petrov–Galerkin (MLPG) method [10], and the boundary element method [11]. In addition, Ciarletta and Sumbatyan [12] examined the reflection of inclined incident plane waves from the free boundary of a porous half-space, thereby contributing to the understanding of wave propagation in elastic solids with voids. Furthermore, rectangular domains containing micropores have been successfully simulated using open-source software [13], while Chen et al. [14] provided a comprehensive overview of recent advances in functionally graded (FG) porous structures.

Contact mechanics is a fundamental branch of solid mechanics concerned with the stresses, deformations, and interactions that arise when two or more bodies come into contact. Beyond homogeneous elastic solids, contact theory has been extended to layered systems, anisotropic media, viscoelastic solids, and porous materials. The presence of microstructural features such as voids or inclusions can significantly influence the effective stiffness and stress transfer mechanisms within a material. Consequently, classical elasticity solutions may fail to accurately predict the contact response of advanced engineering materials, thereby necessitating the adoption of generalized continuum theories. Poroelastic contact problems in a half-space have been investigated by Pompei et al. [15], Scalia and Sumbatyan [16], Ieşan and Nappa [17], and Selvadurai and Samea [18]. Plane and axisymmetric contact problems of a porous layer resting on a Winkler-type foundation were examined by Chebakov and Kolosova [19, 20], respectively. Furthermore, Chebakov et al. [21] analyzed the contact problem of a linear elastic layer bonded to a porous half-plane. The indentation of a half-space by a spherical punch was studied within the framework of Biot's theory by Liu and Huang [22]. In addition, Samea and Selvadurai [23] investigated the axisymmetric indentation of a poroelastic half-plane coated with an inextensible layer located at a finite depth and subjected to loading by a rigid indenter. More recently, Chebakov and Kolosova [24] examined a two-dimensional contact problem between a rigid stamp and a poroelastic rectangular domain resting on a rigid foundation.

Based on the foregoing literature review, it is evident that frictionless contact problems in porous media have been widely investigated. Nevertheless, to the best of the authors' knowledge, the frictional contact behavior of porous elastic materials has not yet been addressed in the open literature. Motivated by this gap, the present study examines the frictional contact response of a porous elastic layer subjected to indentation by a rigid cylindrical punch. The linear elastic behavior of the porous medium containing voids is modeled within the framework of the Cowin–Nunziato micro-dilatation theory. By employing the Fourier transform technique, the governing equations of the two-dimensional contact problem are reduced to a Cauchy-type singular integral equation of the second kind. The resulting singular integral equation is then solved numerically using the Gauss–Jacobi quadrature method.

2 Formulation of the problem

The geometry of the plane strain contact problem of a porous layer with height h, fully fixed to a rigid base, is illustrated in Fig. 1. The porous layer is subjected to a normal force P acting in the vertical direction and tangential force $Q = \eta P$ acting in the tangential direction through a rigid cylindrical punch of radius R, where η denotes the coefficient of friction.

The equilibrium equations in the absence of body forces are given by:

$$\frac{\partial \sigma_x}{\partial x} + \frac{\partial \tau_{xy}}{\partial y} = 0 \tag{1a}$$

$$\frac{\partial \tau_{xy}}{\partial x} + \frac{\partial \sigma_y}{\partial y} = 0 \tag{1b}$$

For the porous layer, the stress-displacement relations can be written as:

$$\sigma_x = \frac{\mu}{(\kappa - 1)}\left((1+\kappa)\frac{\partial u}{\partial x} + (3-\kappa)\frac{\partial v}{\partial y} + H(1+\kappa)\Phi\right) \tag{2a}$$

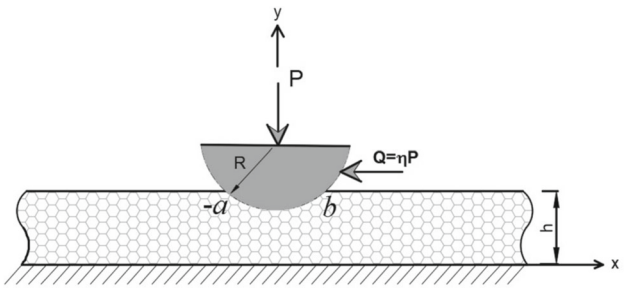

Fig. 1 Geometry of the porous medium under a frictional cylindrical punch

$$\sigma_y = \frac{\mu}{(\kappa-1)}\left((3-\kappa)\frac{\partial u}{\partial x} + (1+\kappa)\frac{\partial v}{\partial y} + H(1+\kappa)\Phi\right) \tag{2b}$$

$$\tau_{xy} = \mu\left(\frac{\partial u}{\partial y} + \frac{\partial v}{\partial x}\right) \tag{2c}$$

The constitutive equations for homogeneous linear elastic and porous elastic materials are expressed as:

$$(1+\kappa)\frac{\partial^2 u}{\partial x^2} + (\kappa-1)\frac{\partial^2 u}{\partial y^2} + 2\frac{\partial^2 v}{\partial x \partial y} + H(1+\kappa)\frac{\partial \Phi}{\partial x} = 0 \tag{3a}$$

$$(\kappa-1)\frac{\partial^2 v}{\partial x^2} + (1+\kappa)\frac{\partial^2 v}{\partial y^2} + 2\frac{\partial^2 u}{\partial x \partial y} + H(1+\kappa)\frac{\partial \Phi}{\partial x} = 0 \tag{3b}$$

$$l_1^2\left(\frac{\partial^2 \Phi}{\partial x^2} + \frac{\partial^2 \Phi}{\partial y^2}\right) - \frac{l_1^2}{l_2^2}\Phi - \left(\frac{\partial u}{\partial x} + \frac{\partial v}{\partial y}\right) = 0 \tag{3c}$$

The dimensionless parameters appearing in these equations are defined as:

$$\kappa = 3-4\nu,\ H = \frac{(1+\nu)(1-2\nu)}{E(1-\nu)}\beta,\ l_1^2 = \frac{\alpha}{\beta},\ l_2^2 = \frac{\alpha}{\xi} \tag{4}$$

where $E\,[N/m^2]$ is the elasticity modulus, ν is Poisson's ratio, $\alpha\,[N]$ is the void/pore diffusion parameter, $\xi\,[N/m^2]$ is the void stiffness modulus, $\beta\,[N/m^2]$ is the void coupling parameter, and Φ represents the change in the volume fraction of pores. Note that, the parameter β can be computed in terms of the coupling parameter ($N\,[+]$) as:

$$\beta = \sqrt{\frac{N\xi E(\nu-1)}{-1+\nu+2\nu^2}},\ 0 \le N \le 1 \tag{5}$$

Since Eq. (3) consist of partial differential equations, the Fourier integral transform technique is employed to reduce them to ordinary differential equations. The exponential Fourier transforms of the unknown functions with respect to the coordinate are x defined as:

$$\{\, u(x,y),\ v(x,y), \Phi(x,y)\,\} = \int_{-\infty}^{\infty} \{\, \tilde{u}(\omega,y),\ \tilde{v}(\omega,y),\ \tilde{\Phi}(\omega,y)\}\, e^{-i\omega x} d\omega \tag{6}$$

where $\tilde{u}(\omega,\ y)$, $\tilde{v}(\omega,\ y)$ and $\tilde{\Phi}(\omega,\ y)$ denote the Fourier transforms of the displacement components and change in volume fraction, respectively; ω is the transform variable and i is the imaginary unit. Substituting Eq. (6) into Eq. (3) yields the following ordinary differential equations:

$$(1+)(1+\kappa)\omega^2\tilde{u} + iH(1+\kappa)\omega\tilde{\Phi} + 2i\omega\frac{d\tilde{v}}{dy} + (1-\kappa)\frac{\partial^2\tilde{u}}{\partial y^2} = 0 \tag{7a}$$

$$(1-\kappa)\omega^2\frac{d\tilde{v}}{dy} - 2i\omega\frac{d\tilde{u}}{dy} + (1+\kappa)H\left(\frac{d\tilde{\Phi}}{dy} + \frac{d^2\tilde{v}}{dy^2}\right) = 0 \tag{7b}$$

$$i\omega\tilde{u} - \frac{l_1^2(1+l_2^2\omega^2)}{l_2^2}\tilde{\Phi} - \frac{d\tilde{v}}{dy} + l_1^2\frac{d^2\tilde{\Phi}}{dy^2} = 0 \tag{7c}$$

Solving the system (7), the characteristic polynomial is obtained as:

$$(n^2-\omega^2)^2\left(H\,l_2^2 + l_1^2\left(-1 + l_2^2\left(n^2-\omega^2\right)\right)\right) = 0 \tag{8}$$

The roots of the characteristic Eq. (8) are denoted by n_j ($j = 1, 2, ..., 4$). Accordingly, the general solution for $\tilde{u}$,$\tilde{w}$ and $\tilde{\Phi}$ can be can be expressed in terms of these roots as:

$$\tilde{u}(\omega, y) = A_1 e^{\omega y} + A_2 y e^{\omega y} + A_3 e^{-\omega y} + A_4 y e^{-\omega y} + A_5 e^{my} + A_6 e^{-my} \tag{9}$$

where the coefficients are defined by:

$$m = \frac{\sqrt{l_1^2 - H\,l_2^2 + l_1^2 l_2^2\omega^2}}{l_1 l_2} \tag{10}$$

After determining the displacement component $\tilde{u}(\omega,\ y)$, the following expressions maybe obtained for $\tilde{v}(\omega,\ y)$ and $\tilde{\Phi}(\omega,\ y)$:

$$\tilde{v}(\omega, y) = i\left(A_1 e^{\omega y} + A_2(y+k_1)e^{\omega y} - A_3 e^{-\omega y} + A_4(k_1 - y)e^{-\omega y} + A_5 e^{my}\frac{m}{\omega} - A_6 e^{-my}\frac{m}{\omega}\right) \tag{11}$$

$$\tilde{\Phi}(\omega, y) = -i\left(2A_2 k_2 e^{\omega y} - 2A_4 k_2 e^{-\omega y} - A_5 k_3 e^{my} - A_6 k_3 e^{-my}\right) \tag{12}$$

Substituting the inverse Fourier transforms of the displacement components and the change in the volume fraction—containing unknown constants—into Eq. (2), the stresses can be written in terms of their Fourier transforms as:

$$\begin{aligned}\tilde{\sigma}_x(\omega, y) = 2\mu i\big(&-A_1\omega\, e^{\omega y} + A_2(k_4 - y\omega)e^{\omega y} - A_3\omega\, e^{-\omega y} - A_4(k_4 + y\omega)e^{-\omega y}\,0 \\ &- A_5\frac{m^2}{\omega}e^{my} - A_6\frac{m^2}{\omega}e^{-my}\Big)\end{aligned} \tag{13a}$$

$$\begin{aligned}\tilde{\sigma}_y(\omega, y) = 2\mu i\big(&A_1\omega\, e^{\omega y} - A_2(k_5 - y\omega)e^{\omega y} + A_3\omega\, e^{-\omega y} + A_4(k_5 + y\omega)e^{-\omega y} \\ &+A_5\omega e^{my} + A_6\omega e^{-my}\big)\end{aligned} \tag{13b}$$

$$\begin{aligned}\tilde{\tau}_{xy}(\omega, y) = 2\mu\big(&A_1\omega\, e^{\omega y} - A_2(k_6 - y\omega)e^{\omega y} - A_3\omega\, e^{-\omega y} - A_4(k_6 + y\omega)e^{-\omega y} \\ &+A_5 m e^{my} - A_6 m e^{-my}\big)\end{aligned} \tag{13c}$$

The coefficients k_i ($i = 1, 2..., 6$) are given in the Appendix. A_j ($j = 1, 2..., 6$) are the unknowns, and they will be determined from the boundary conditions of the problem.

3 The boundary conditions and the singular integral equation

The unknown coefficients A_j ($j = 1, 2..., 6$) appearing in the displacement field, stress components and change in the volume fraction of pores are determined from the following boundary conditions:

$$\sigma_y(x, h) = \begin{cases} -p(x) & -a < x < b \\ 0 & x \le -a,\ x \ge b \end{cases} \tag{14a}$$

$$\tau_{xy}(x, h) = \begin{cases} -\eta\, p(x) & -a < x < b \\ 0 & x \le -a,\ x \ge b \end{cases} \tag{14b}$$

$$u(x, 0) = 0 \tag{14c}$$

$$v(x, 0) = 0 \tag{14d}$$

$$\frac{\partial\Phi(x, h)}{\partial y} = 0 \tag{14e}$$

$$\frac{\partial \Phi(x,0)}{\partial y} = 0 \tag{14f}$$

Here, $p(x)$ denotes the contact stress in the contact region $(-a,\ b)$ between the rigid cylindrical punch and the porous layer, and η is the coefficient of friction.

Applying the Fourier transform to the boundary conditions (14) results in a system of six linear algebraic equations. Solving this system yields the unknown coefficients in terms of the unknown contact stress:

$$A_j = \int_{-a}^{a} p(t) e^{i\omega t} (A_j^p + \eta\, A_j^q) dt \quad j = 1, 2..., 6 \tag{15}$$

Although the coefficients are formally obtained, the contact stress $p(x)$ remains unknown. Since the punch is rigid, the deformation of the porous layer beneath the punch must conform to the punch profile. This physical compatibility condition leads to the following additional mixed boundary condition:

$$\frac{\partial v(x,h)}{\partial x} = \frac{x}{R} \quad -a < x < b \tag{16}$$

By substituting the unknowns A_j determined by Eq. (15) into the mixed condition (16), a Cauchy-type singular integral equation of the second kind is obtained:

$$\eta\phi_2 p(x) + \frac{1}{\pi} \int_{-a}^{b} p(t) dt \left[\frac{\phi_1}{t-x} + T_1(x,t) + \eta\, T_2(x,t) \right] = \frac{x}{R} \quad (-a < x < b) \tag{17}$$

where the kernel functions are defined Eqs. (18a–d)

$$T_1(x,t) = \int_0^{\infty} (\ S_1(\omega) - \phi_1) \sin\omega(t-x) d\omega \tag{18a}$$

$$T_2(x,t) = \int_0^{\infty} (\ S_2(\omega) - \phi_2) \cos\omega(t-x) d\omega \tag{18b}$$

$$S_1(\omega) = \omega \sum_{j=1}^{4} A_j^p m_j, \quad S_2(\omega) = -i\omega \sum_{j=1}^{4} A_j^q m_j \tag{18c}$$

$$\phi_1 = \lim_{\omega\to\infty}\ S_1(\omega), \quad \phi_2 = \lim_{\omega\to\infty}\ S_2(\omega) \tag{18d}$$

To complete the formulation, the contact width must satisfy the global equilibrium condition:

$$\int_{-\infty}^{\infty} \sigma_y(x,h) dx = -\int_{-a}^{b} p(t) dt = -P \tag{19}$$

4 Numerical solution of the singular integral equation

Introducing the normalization:

$$t = \frac{a+b}{2} r + \frac{b-a}{2}, \quad x = \frac{a+b}{2} s + \frac{b-a}{2} \tag{20}$$

the transforms Eq. (17) in to the following form dimensionless form:

$$\eta\phi_2 p(s) + \frac{1}{\pi} \int_{-1}^{1} p(r) dr \left[\frac{\phi_2}{r-s} + T_1^*(s,r) + \eta\, T_2^*(s,r) \right] = \frac{1}{R} \left(\frac{a+b}{2} s + \frac{b-a}{2} \right) \tag{21}$$

where

$$T_1^*(s,r) = \frac{a+b}{2} T_1(x,t), \quad T_2^*(s,r) = \frac{a+b}{2} T_2(x,t) \tag{22}$$

As a result of the normalization, the equilibrium Eq. (19) takes the following form:

$$\frac{a+b}{2} \int_{-1}^{1} p(r)dr = P \tag{23}$$

Because the contact stress vanishes smoothly at the ends of the contact region, the index of the integral Eq. (21) is − 1 [25]. Accordingly, the solution can be expressed in the form:

$$p(r) = g(r)(1-r)^{\Omega_1}(1+r)^{\Omega_2} \tag{24}$$

where $g(r)$ is an unknown bounded function and

$$\Omega_1 = \frac{1}{2\pi i} \ln\left[\frac{\eta\,\phi_2/\phi_1 - i}{\eta\,\phi_2/\phi_1 + i}\right] + N_0 \tag{25a}$$

$$\Omega_2 = \frac{1}{2\pi i} \ln\left[\frac{\eta\,\phi_2/\phi_1 - i}{\eta\,\phi_2/\phi_1 + i}\right] + M_0 \tag{25b}$$

where N_0 and M_0 are arbitrary (positive, zero, or negative) integers and can be determined depending on the physics of the problem.

The singular integral Eq. (21) is discretized using the Gauss–Jacobi integration formulas [25]:

$$\sum_{i=1}^{M} W_i^M g(r_i)\left[\frac{1}{r_i - s_k} + T_1^*(s_k, r_i) + \eta\, T_2^*(s_k, r_i)\right] = \frac{1}{R}\left(\frac{a+b}{2} s_k + \frac{b-a}{2}\right) \quad k = 1, 2..., N+1 \tag{26}$$

The equilibrium condition (23) becomes

$$\frac{a+b}{2} \sum_{i=1}^{N} W_i^M g(r_i) = \frac{P}{\pi} \tag{27}$$

where r_i, s_k and W_i^M are the roots and weighting constants of the Jacobi polynomials defined in Eqs. (8a–c)

$$P_M^{(\Omega_1,\Omega_2)}(r_i) = 0 \quad i = 1, 2, ..., M \tag{28a}$$

$$P_{M-1}^{(-\Omega_1,-\Omega_2)}(s_k) = 0 \quad k = 1, 2, ..., M-1 \tag{28b}$$

$$W_i^M = -\frac{1}{\pi} \frac{(2N + \Omega_1 + \Omega_2 + 2)}{(M+1)!} \frac{\Gamma(M+\Omega_1+1)\Gamma(M+\Omega_2+1)}{\Gamma(M+\Omega_1+\Omega_2+2)} \frac{2^{(\Omega_1+\Omega_2)}}{P_M^{(\Omega_1,\Omega_2)\prime}(r_i) P_{M+1}^{(\Omega_1,\Omega_2)}(r_i)} \tag{28c}$$

Equation (26) and Eq. (27) give $N+2$ algebraic equations to determine $N+2$ unknowns which are $g(r_m)$ ($m = 1, ..., N$), and the contact areas "a,b". Since the system is nonlinear with respect to the contact width, an iterative scheme is employed to determine the unknown contact region.

5 Classical solution of the contact problem

In the classical solution, displacement and stress components for the non-porous layer can be written as follows (Çömez and Erdöl [2013])

$$u(x,y) = \frac{1}{2\pi}\int_{-\infty}^{\infty}\left[(C_1+C_2y)\,e^{-\omega y}+(C_3+C_4y)\,e^{\omega y}\right]e^{-i\omega x}d\omega \tag{29a}$$

$$v(x,y) = -\frac{1}{2\pi}i\int_{-\infty}^{\infty}\left[\left[C_1+\left(\frac{\kappa}{\omega}+y\right)C_2\right]e^{-\omega y}+\left[-C_3+\left(\frac{\kappa}{\omega}-y\right)C_4\right]e^{\omega y}\right]e^{-i\omega x}d\omega \tag{29b}$$

$$\frac{\sigma_x(x,y)}{2\mu} = -\frac{1}{2\pi}i\int_{-\infty}^{\infty}\omega\left[C_1e^{-\omega y}+\left(\frac{\kappa-3}{2\omega}+y\right)C_2e^{-\omega y}+C_3e^{\omega y}+\left(y-\frac{\kappa-1}{2\omega}\right)C_4e^{\omega y}\right]e^{-i\omega x}d\omega \tag{29c}$$

$$\frac{\sigma_y(x,y)}{2\mu} = \frac{1}{2\pi}i\int_{-\infty}^{\infty}\omega\left[C_1e^{-\omega y}+\left(\frac{\kappa+1}{2\omega}+y\right)C_2e^{-\omega y}+C_3e^{\omega y}+\left(y-\frac{\kappa+1}{2\omega}\right)C_4e^{\omega y}\right]e^{-i\omega x}d\omega \tag{29d}$$

$$\frac{\tau_{xy}(x,y)}{2\mu} = -\frac{1}{2\pi}\int_{-\infty}^{\infty}\omega\left[C_1e^{-\omega y}+\left(\frac{\kappa-1}{2\omega}+y\right)C_2e^{-\omega y}-C_3e^{\omega y}-\left(y-\frac{\kappa-1}{2\omega}\right)C_4e^{\omega y}\right]e^{-i\omega x}d\omega \tag{29e}$$

Applying the boundary conditions (14a–d) and (16) following singular integral eqution can be obtained

$$\eta\beta_4\,p(x)+\frac{1}{\pi}\int_{-a}^{b}p(t)dt\left[\frac{\beta_3}{t-x}+K_3(x,t)+\eta\,K_4(x,t)\right]=0\quad(-a<x<a) \tag{30}$$

where

$$K_3(x,t) = \frac{(1+\kappa)(2\kappa+e^{2\omega h}(1+4\omega h+4\omega^2h^2+\kappa^2))}{4(\kappa+\kappa e^{4\omega h}+e^{2\omega h}(1+4\omega^2h^2+\kappa^2)} - \beta_3 \tag{31a}$$

$$K_4(x,t) = \frac{e^{2\omega h}(1+\kappa)(-1+4\omega^2h^2+\kappa^2))}{4(\kappa+\kappa e^{4\omega h}+e^{2\omega h}(1+4\omega^2h^2+\kappa^2)} - \beta_4 \tag{31b}$$

$$\beta_3 = -\frac{1+\kappa}{4},\quad \beta_4 = \frac{-1+\kappa}{4},\quad \kappa = 3-4\nu \tag{31c}$$

6 Numerical results

In this section the effect of some quantities such as friction coefficient (η), coupling parameter (N), Poisson's ratio (ν), indentation load (P) and height of layer (h) on the contact stress $p(x)$, in-plane stress $\sigma_x(x,\,h)$ and vertical displacement $v(x,\,h)$ are given. In the following analysis, void/pore diffusion parameter and void stiffness modulus are taken as $\alpha = 0.01N$ and $\xi = 40x10^3N/m^2$, respectively. Based on the numerical investigations conducted, it was observed that variations in the void/pore diffusion parameter and the void stiffness modulus have no significant influence on the contact stresses, vertical displacement, or in-plane stress components. Therefore, graphical results illustrating the effects of these parameters are not presented.

As the coupling parameter approaches zero, the porous model degenerates into the classical elastic model without voids. The contact stress distributions obtained in this limiting case coincide with the corresponding classical solutions available in the literature, thereby validating the correctness of the present formulation. Figure 2 also shows the influence of the punch radius. As the punch radius increases, a larger portion of the punch comes into contact with the layer, resulting in a decrease in both the contact stress and the tensile peaks.

Figure 3 illustrates the influence of the indentation load and the coupling parameter on the contact width. The contact width increases with increasing coupling parameter. This behavior can be attributed to the fact that a larger coupling parameter corresponds to a more porous structure, which allows the layer to deform more

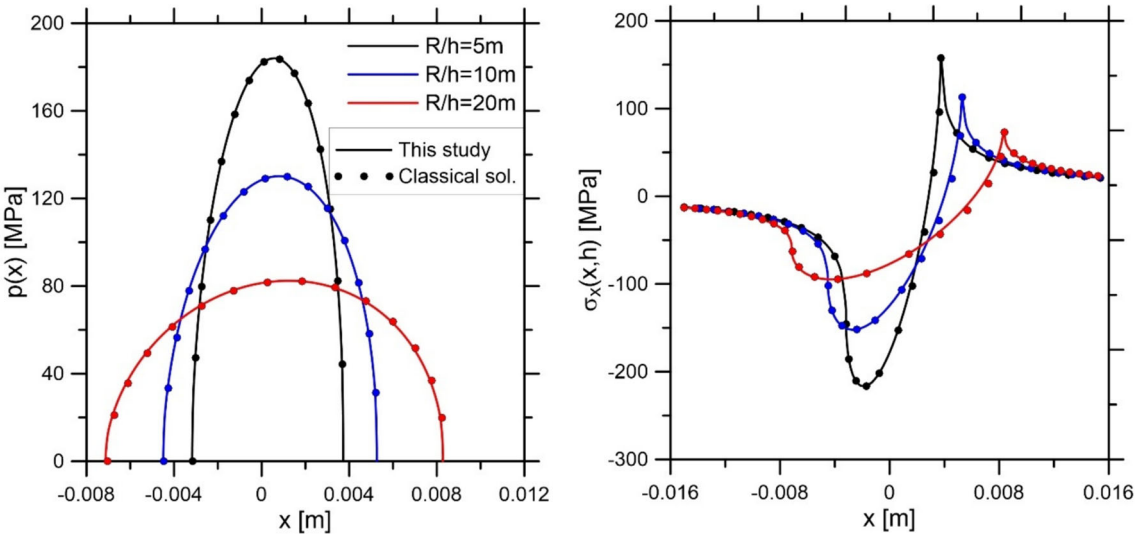

Fig. 2 Comparison of the contact stress and in-plane stress with classical solution. ($P = 1x10^6 N/m$, $h = 0.1m$, $\eta = 0.4$, $\nu = 0.25$, $N = 0.5$, $E = 100x10^9 N/m^2$)

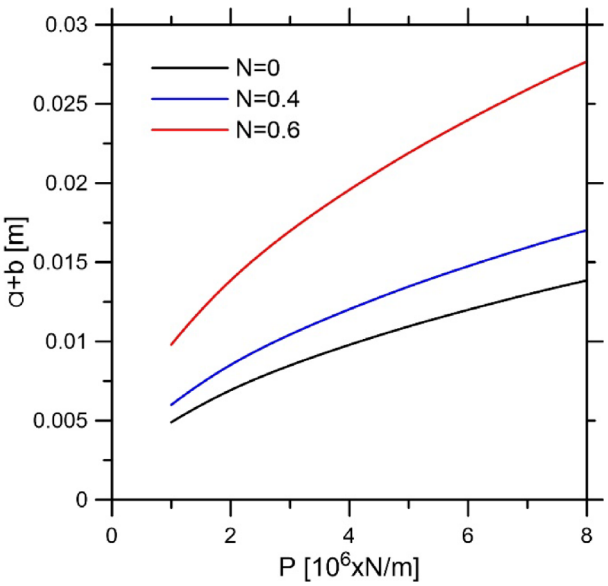

Fig. 3 Variations of the contact width, $a + b$, versus external load, P, and coupling parameter, N. ($R = 1m$, $h = 1m$, $\eta = 0.4$, $\nu = 0.25$)

easily. It is evident that as the indentation load increases, the punch penetrates further into the layer, resulting in an increase in the contact width.

The peak value of the contact stress is independent of the friction coefficient (Fig. 4). In the frictionless case, the contact stress distribution is symmetric. However, the presence of friction breaks this symmetry, and the contact region shifts in the direction opposite to the tangential load. In the absence of friction, tensile stress is almost negligible. However, the tensile peak in the in-plane stress increases considerably as the friction coefficient increases. Stress peaks increase significantly with increasing friction in the contact region, which may lead to surface damage and crack initiation near the trailing edge. Therefore, lower friction coefficients reduce the likelihood of crack initiation and subsequent propagation. In addition, the vertical displacement decreases slightly as the friction coefficient increases.

As the N value, i.e., the porosity parameter, increases, the contact stress decreases due to the reduction in the effective contact stiffness associated with higher porosity (Fig. 5). The vertical displacement in the contact

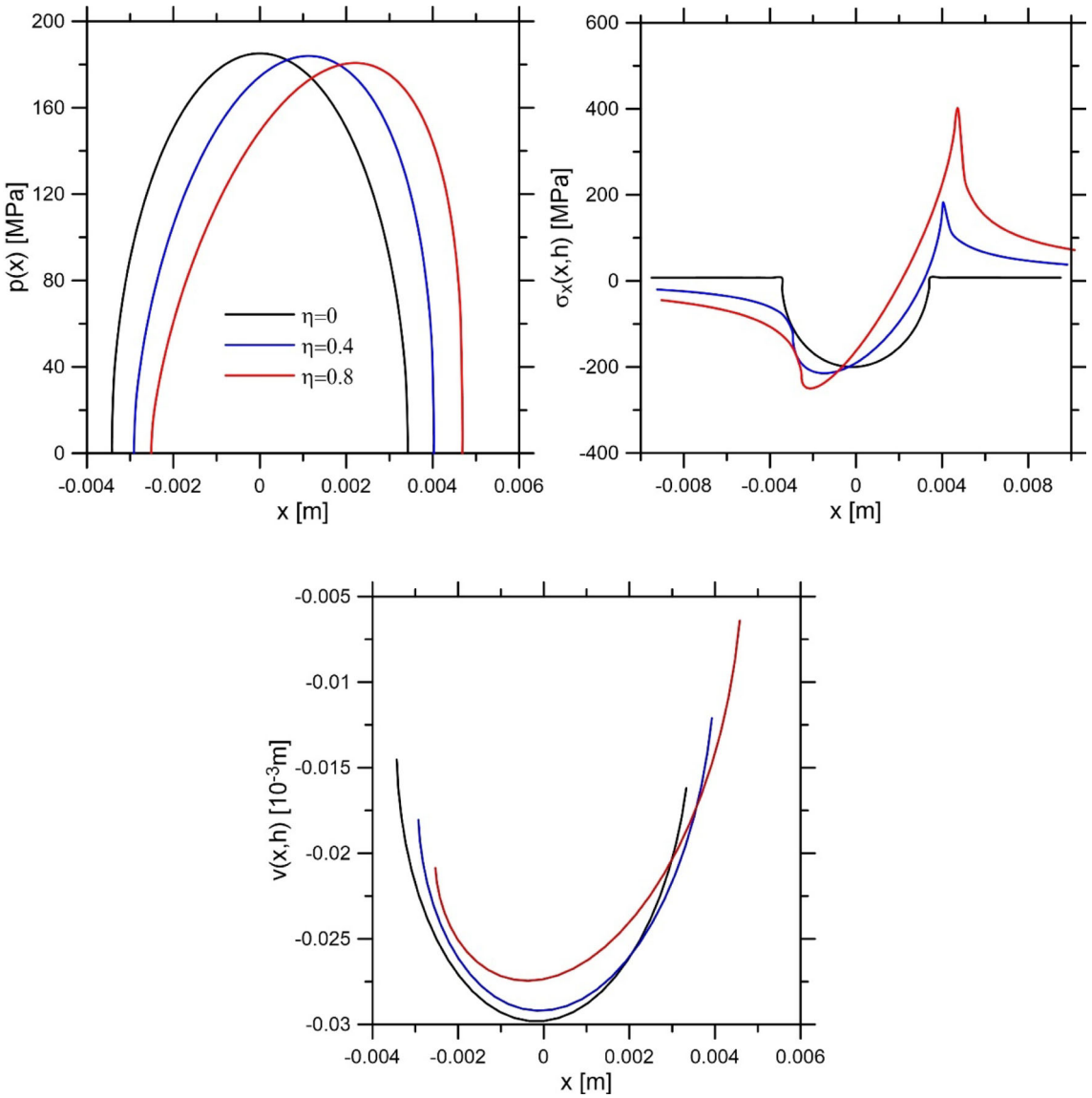

Fig. 4 Variations of the contact stress, $p(x)$, vertical displacement, $v(x,\ h)$, in-plane stress, $\sigma_x(x,\ h)$, versus friction coefficient η. ($P = 1x10^7 N/m,\ R = 10m,\ h = 1m,\ \nu = 0.25,\ E = 200x10^9 GPa,\ N = 0.5$)

region increases with increasing porosity. This is an expected result, since a more porous structure allows greater penetration of the punch, whereas lower porosity makes deformation more difficult.

Figure 6 shows the effect of Poisson's ratio on the contact stress, in-plane stress, and vertical displacement in the contact region. As Poisson's ratio increases, the material becomes less compressible and the layer behaves more tightly. Consequently, the contact stress increases with increasing Poisson's ratio. In addition, the vertical displacement decreases significantly, while the tensile peak in the in-plane stress increases slightly.

Figure 7 shows the variation of the contact stress, in-plane stress, and vertical displacement with the elastic modulus. As expected, an increase in the elastic modulus corresponds to a stiffer layer. With increasing stiffness, the layer's flexibility decreases, resulting in reduced penetration of the punch. Consequently, the contact stress increases with the elastic modulus. In addition, the tensile peak in the in-plane stress increases significantly, while the vertical displacement decreases substantially.

With increasing indentation load, the contact stress, in-plane stress, and vertical displacement all increase. Unlike other parameters, the contact stress and the contact width exhibit a direct correlation with the applied

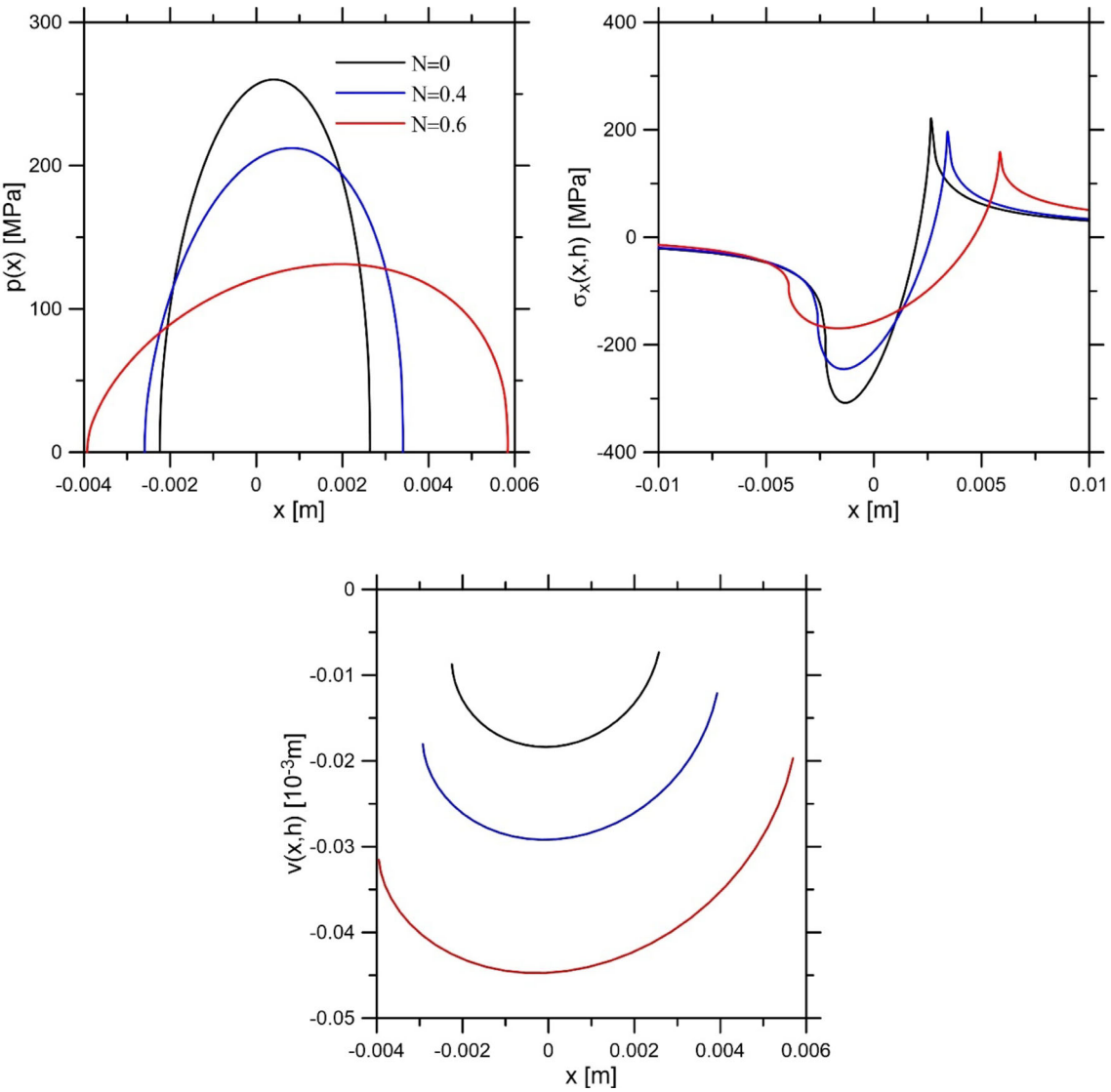

Fig. 5 Variations of the contact stress, $p(x)$, vertical displacement, $v(x,\ h)$, in-plane stress, $\sigma_x(x,\ h)$, versus porosity parameter N. ($P = 1x10^6 N/m,\ R = 1m,\ h = 0.1m,\ \eta = 0.4,\ \nu = 0.25,\ E = 200x10^9 GPa$)

load (Fig. 8). The tensile peak can be reduced by controlling the indentation load, thereby preventing potential surface damage and crack formation.

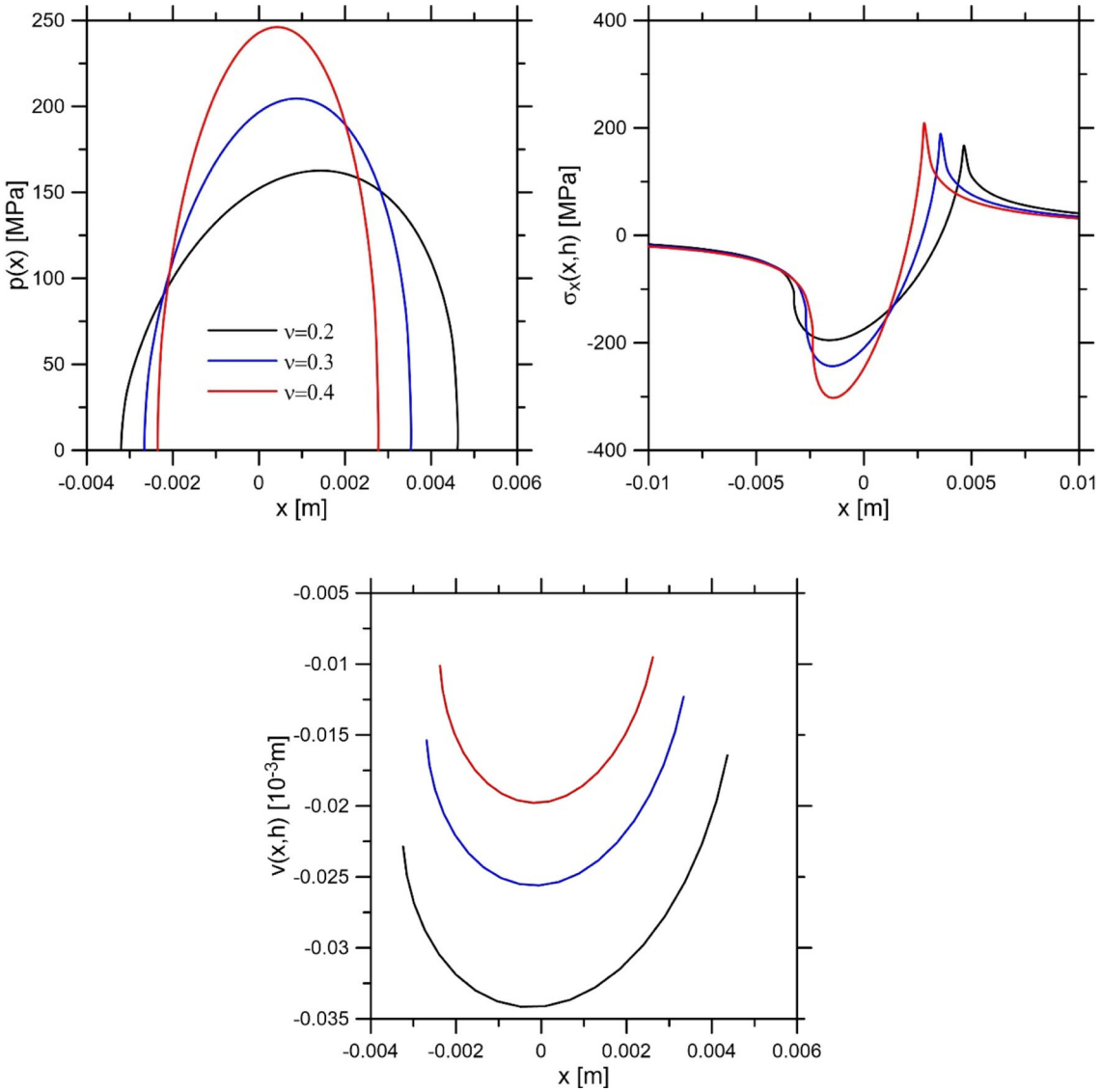

Fig. 6 Variations of the contact stress, $p(x)$, vertical displacement, $v(x,\ h)$, in-plane stress, $\sigma_x(x,\ h)$, versus Poisson's ratio ν.($P = 1x10^6 N/m$, $R = 1m$, $h = 0.1m$, $\eta = 0.4$, $E = 200x10^9 GPa$, $N = 0.5$)

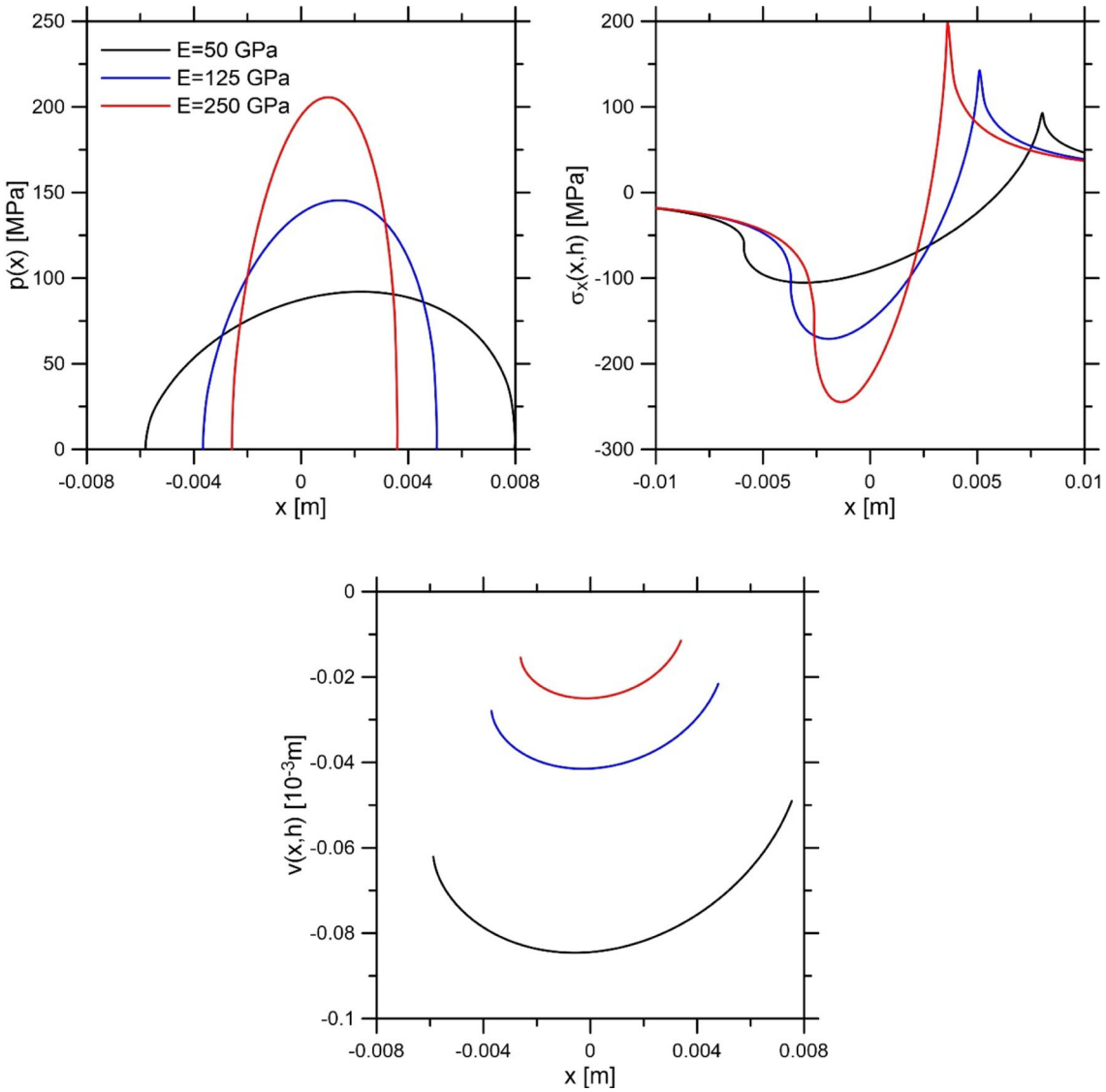

Fig. 7 Variations of the contact stress, $p(x)$, vertical displacement, $v(x,\ h)$, in-plane stress, $\sigma_x(x,\ h)$, versus elasticity modulus E. ($P = 1x10^6 N/m,\ R = 1m,\ h = 0.1m,\ \eta = 0.4,\ \nu = 0.25,\ N = 0.5$)

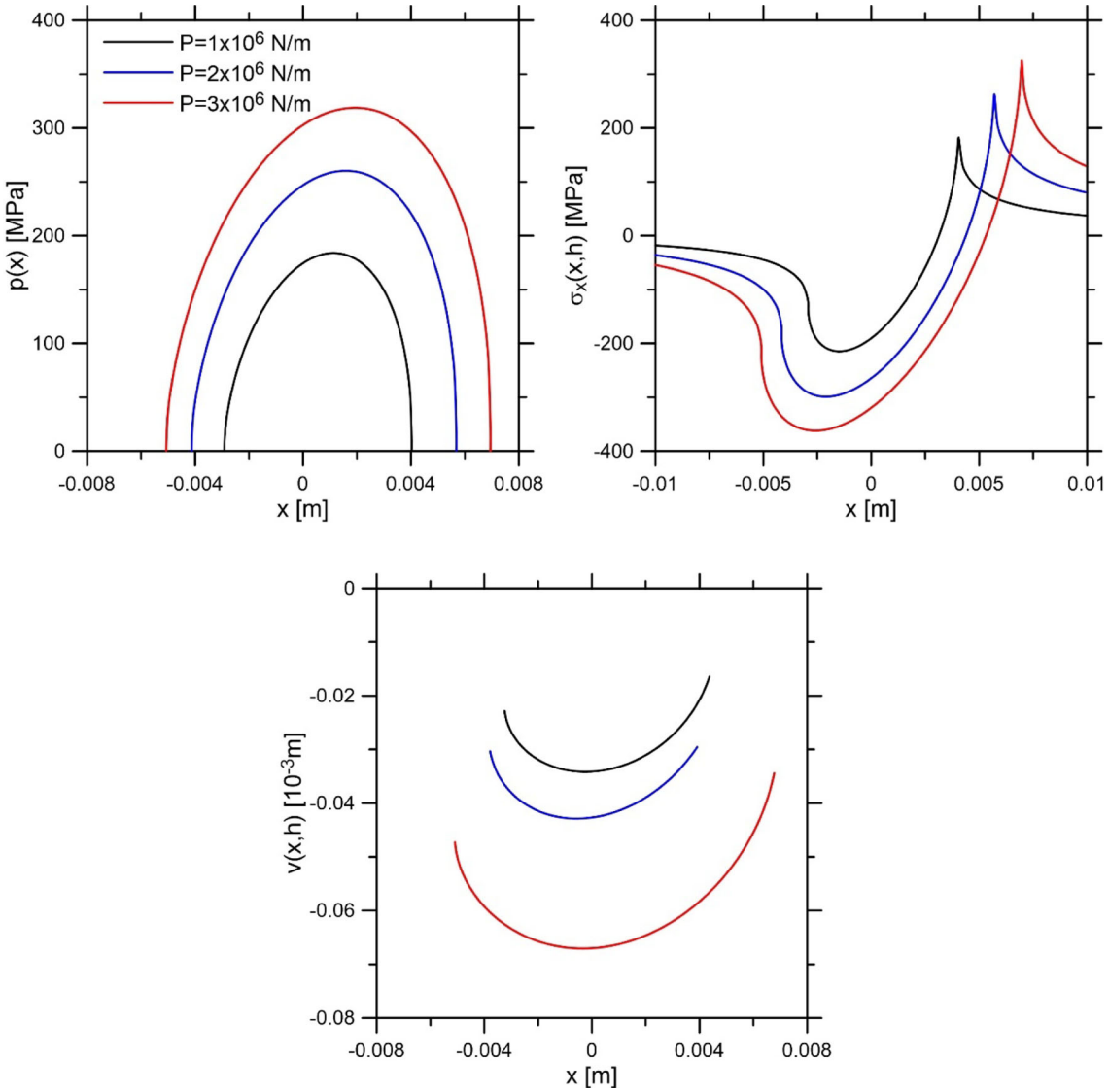

Fig. 8 Variations of the contact stress, $p(x)$, vertical displacement, $v(x,\ h)$, in-plane stress, $\sigma_x(x,\ h)$, versus external load P. ($R = 1m$, $h = 0.1m$, $\eta = 0.4$, $\nu = 0.25$, $E = 200x10^9 GPa$, $N = 0.5$)

7 Conclusion

In this study, the frictional contact problem of a porous layer indented by a rigid flat punch is analytically investigated. The Cowin–Nunziato micro-dilatation theory is employed to incorporate the effects of voids into the linear elastic constitutive behavior of the material. By applying the Fourier transform, the plane contact problem is reduced to a Cauchy-type singular integral equation of the second kind, in which the contact stress is the unknown. The main findings are summarized as follows:

- Increasing friction in the contact region significantly amplifies tensile peaks, potentially causing surface damage and crack formation near the trailing edge. A small coefficient of friction may be chosen to mitigate these risks.
- Increasing the combined parameter N enlarges the void fraction, resulting in a longer contact length and lower contact stress. Maximum vertical displacement occurs at higher values of the coupling parameter due to the reduced material stiffness.
- As Poisson's ratio increases, the material becomes less compressible, and the layer behaves more rigidly. Consequently, the contact stress rises with increasing Poisson's ratio.

- Increasing the layer's stiffness reduces its flexibility, limiting the penetration of the punch. As a result, the contact stress increases with the elastic modulus.

Author contributions İ.Ç. prepared the whole manuscript.

Funding Open access funding provided by the Scientific and Technological Research Council of Türkiye (TÜBİTAK).

Data availability No datasets were generated or analysed during the current study.

Declarations

Competing interests The authors declare no competing interests.

Open Access This article is licensed under a Creative Commons Attribution 4.0 International License, which permits use, sharing, adaptation, distribution and reproduction in any medium or format, as long as you give appropriate credit to the original author(s) and the source, provide a link to the Creative Commons licence, and indicate if changes were made. The images or other third party material in this article are included in the article's Creative Commons licence, unless indicated otherwise in a credit line to the material. If material is not included in the article's Creative Commons licence and your intended use is not permitted by statutory regulation or exceeds the permitted use, you will need to obtain permission directly from the copyright holder. To view a copy of this licence, visit http://creativecommons.org/licenses/by/4.0/.

Appendix

Expressions of the coefficients k_i $(i = 1, 2...6)$ appearing in (10) are given below.

$$k_1 = \frac{-2l_1^2\kappa + Hl_2^2(1+\kappa)}{(2l_1^2 - Hl_2^2(1+\kappa))\omega}, \quad k_2 = \frac{l_2^2(-1+\kappa)}{2l_1^2 - Hl_2^2(1+\kappa)}, \quad k_3 = \frac{l_1^2 - Hl_2^2}{Hl_1^2 l_2^2 \omega} \tag{32}$$

$$k_4 = \frac{l_1^2(-3+\kappa) + Hl_2^2(1+\kappa)}{2l_1^2 - Hl_2^2(1+\kappa)}, \quad k_5 = \frac{(l_1^2 - Hl_2^2)(1+\kappa)}{2l_1^2 - Hl_2^2(1+\kappa)}, \quad k_6 = \frac{l_1^2(-1+\kappa)}{2l_1^2 - Hl_2^2(1+\kappa)} \tag{33}$$

References

1. Biot, M.A., Willis, D.G.: The elastic coefficients of the theory of consolidation. J. Appl. Mech. **24**(Dec), 594–601 (1957)
2. Mindlin, R.D.: Microstructure in linear elasticity. Arch. Ration. Mech. Anal. **16**, 51–78 (1963)
3. Nunziato, J.W., Cowin, S.C.: A nonlinear theory of elastic materials with voids. Arch. Ration. Mech. Anal. **72**, 175–201 (1979)
4. Cowin, S.C., Nunziato, J.W.: Linear elastic materials with voids. J. Elast. **13**, 125–147 (1983)
5. Bishay, P.L., Repka, M., Sladek, V., Sladek, J.: On the characterization of porosity-related parameters in micro-dilatation theory. Acta Mech. **228**(5), 1631–1644 (2017)
6. Repka, M., Sládek, V., Sládek, J.: Numerical analysis of poro-elastic materials described by the micro-dilatation theory. Procedia Eng. **190**, 248–254 (2017)
7. Lurie, S.A., Kalamkarov, A.L., Solyaev, Y.O., Ustenko, A.D., Volkov, A.V.: Continuum micro-dilatation modeling of auxetic metamaterials. Int. J. Solids Struct. **132**, 188–200 (2018)
8. Lurie, S., Solyaev, Y., Volkov, A., Volkov-Bogorodskiy, D.: Bending problems in the theory of elastic materials with voids and surface effects. Math. Mech. Solids **23**(5), 787–804 (2018)
9. Bishay, P.L., Sladek, J., Sladek, V., Gao, X.W.: Analysis of elastic media with voids using a mixed-collocation finite-element method. J. Eng. Mech. **143**(4), 04016119 (2017)
10. Sladek, J., Sladek, V., Repka, M., Bishay, P.L.: Static and dynamic behavior of porous elastic materials based on micro-dilatation theory: a numerical study using the MLPG method. Int. J. Solids Struct. **96**, 126–135 (2016)
11. Leroy, J.E., Popov, V.L.: Boundary element method for normal contacts of poroelastic layers. Int. J. Solids Struct. (2026). https://doi.org/10.1016/j.ijsolstr.2026.113866
12. Ciarletta, M., Sumbatyan, M.A.: Reflection of plane waves by the free boundary of a porous elastic half-space. J. Sound Vib. **259**(2), 253–264 (2003)
13. Arman, A., Eso, R.: The finite element method for the elasticity of micro-pores material. WSEAS Trans. Adv. Eng. Educ. **21**, 72–79 (2024)
14. Chen, D., Gao, K., Yang, J., Zhang, L.: Functionally graded porous structures: analyses, performances, and applications–a review. Thin-Walled Struct. **191**, 111046 (2023)
15. Pompei, A., Rigano, A., Sumbatyan, M.A.: Contact problem for a rectangular punch on the porous elastic half-space. J. Elast. **76**(1), 1–19 (2004)

16. Scalia, A., Sumbatyan, M.A.: Contact problem for porous elastic half-plane. J. Elast. Phys. Sci. Solids **60**(2), 91–102 (2000)
17. Ieşan, D., Nappa, L.: Axially symmetric problems for a porous elastic solid. Int. J. Solids Struct. **40**(20), 5271–5286 (2003)
18. Selvadurai, A.P.S., Samea, P.: On the indentation of a poroelastic halfspace. Int. J. Eng. Sci. **149**, 103246 (2020)
19. Chebakov, M.I., Kolosova, E.M.: Contact interaction of a stamp and a poroelastic strip lying on a winkler base. Mech. Compos. Mater. **59**(6), 1169–1180 (2024a)
20. Chebakov, M.I., Kolosova, E.M.: Axisymmetrical problem on interaction of a stamp and a poroelastic layer lying on a winkler base. Mech. Compos. Mater. **60**(5), 969–976 (2024b)
21. Chebakov, M., Kolosova, E., Iankov, R., Datcheva, M.: Contact problem for a rigid flat stamp and a linear elastic strip bonded to porous half-plane. J. Theor. and Appl. Mech. (Bulgaria) **51**, 391–404 (2021)
22. Liu, M., Huang, H.: Poroelastic response of spherical indentation into a half space with a drained surface via step displacement. Int. J. Solids Struct. **165**, 34–49 (2019)
23. Samea, P., Selvadurai, A.P.S.: A contact problem for a poroelastic halfspace containing an embedded inextensible membrane. Int. J. Numer. Anal. Methods Geomech. **44**(16), 2167–2188 (2020)
24. Chebakov, M.I., Kolosova, E.M.: Contact interaction of stamp and poroelastic rectangle. Mech. Compos. Mater. **61**, 1–8 (2026)
25. Erdogan, F.: Mixed boundary value problems in mechanics. In: Nemat-Nasser, S. (ed.) Mechanics today, vol. 4. Pergamon Press, Oxford (1978)
26. Çömez, İ., Erdöl, R. Frictional contact problem of a rigid stamp and an elastic layer bonded to a homogeneous substrate. Arch. Appl. Mech. **83**(1), 15-24 (2013)

Publisher's Note Springer Nature remains neutral with regard to jurisdictional claims in published maps and institutional affiliations.